RSC Advances

ROYAL SOCIETY OF CHEMISTRY

www.rsc.org/advances

Cite this: DOI: 10.1039/c0xx00000x

www.rsc.org/xxxxxx

ARTICLE TYPE

Rigid Three-Dimensional Ni_3S_4 Nanosheet Frames: Controlled Synthesis and Their Enhanced Electrochemical Performance

Lina Wang,[a] Jiajia Liu,*[a] Li Li Zhang,[b] Baosong Dai,[a] Meng Xu,[a] Muwei Ji,[a] X. S. Zhao,[c] Chuanbao Cao,[a] Jiatao Zhang,*[a] and Hesun Zhu[a]

Received (in XXX, XXX) Xth XXXXXXXXX 20XX, Accepted Xth XXXXXXXXX 20XX
DOI: 10.1039/b000000x

Rigid three-dimensional (3D) Ni_3S_4 nanosheet frames assembled from ultrathin nanosheets are synthesized via a facile solvothermal method. Compared to the flat Ni_3S_4 sheets, the 3D Ni_3S_4 nanosheet frames have both high free volume and high compressive strength. They can deliver very high specific capacitance of 1213 F g^{-1} with good rate performance. In addition, these 3D Ni_3S_4 nanosheet frames are stabilized by plastically deformed ridges. The stabilized nanosheet frames do not unfold or collapse during electrochemical test and thus enhancing their cycling ability.

Nowadays, metal chalcogenide materials have attracted tremendous attention in the field of energy due to their high theoretical capacitance and low cost.[1] Key to their further development in these areas has been the improved surface area and rigidity in their structure.[2] Two-dimensional (2D) metal chalcogenide nanocrystals have provided a much higher specific surface area as compared with their bulk counterparts, which is beneficial to energy devices because the reaction/interaction between the devices and the interacting media can be significantly enhanced.[3] However, during electrode fabrication process, the nanosheet-like materials, such as graphene, tend to aggregate or restack due to strong inter sheet van der Waals attraction.[4] Consequently, many of the unique properties that individual sheets possess, such as high specific surface area and peculiar electron transport behaviours, are significantly compromised or even unavailable in assembly. An efficient strategy to prevent nanosheets aggregation and thus to improve the energy storage performance of sheet-like materials is to synthesize three-dimensional (3D) architectures assembled with nanosheets, such as fabricating sandwich type structures by introducing "spacer" (e.g. carbon nanotubes, nanoparticles)[5] and forming 3D macroporous structures.[6] For instance, Luo *et al.*[7] crumpled the graphene sheets into paper ball-like, fractal-dimensional particles to make them aggregation-resistant in both solvent and solid state, even after mechanical compression. Therefore, the preparation of large-area, aligned nanoporous nanostructured film in a highly crystalline state with well-oriented frameworks, excellent accessibility, and controlled porosity is an effective way to prepare metal chalcogenide based electrode materials.

As an important class of transition metal chalcogenides, nickel sulphides with controlled morphology is of great interest due to their potential applications in hydrogenation catalysts, and electrode materials.[8] The electrochemical performances of the electrode materials are strongly dependent on their sizes, morphologies, and structures; up to now, progress has been made on nickel sulphide based electrodes. For example, Hou *et al.*[9] first investigated the potential application of NiS nanoparticles as a supercapacitor electrode and proposed an electrochemical reaction mechanism. Subsequently, Zhu *et al.*[10] reported the synthesis of hierarchical NiS hollow spheres by an template-engaged conversion method. Due to the unique structural features and high surface area, these NiS hollow spheres show high specific capacitance of 583-927 F g^{-1} at various currents densities of 4.08-10.2 A g^{-1}. Later, Yang *et al.*[11] synthesized a hierarchial flower-like β -NiS electrode with high specific discharge capacitance of 857.76 F g^{-1}. Recently, Pang *et al.*[12] reported the synthesis of uniform NiS_2 nanocubes, and these NiS_2 nanocube electrodes showed a large specific capacitance (695 F g^{-1} at 1.25 A g^{-1}) and excellent cycling performance. However, Ni_3S_4 has attracted much less attention compared to other binary nickel sulfides, such as NiS, Ni_3S_2, and NiS_2, due to the synthetic challenges in obtaining the single phase Ni_3S_4.[13] Ni_3S_4 has cubic spinel structure and is found in nature as the mineral polydymite.[14] Many efforts have been devoted in order to obtain the single-phase Ni_3S_4 efficiently in laboratories. Through selective control of the reaction conditions, such as Ni precursor or capping agents, it is possible to obtain single phase Ni_3S_4 triangular nanoprisms, and nanopyramids.[15] Despite the success in the synthesis of various morphologies, the preparation of uniform 3D Ni_3S_4 nanosheet structure in a highly crystalline state still remains as significant challenge.

Herein, we present a facile, one-pot solvothermal route to prepare rigid 3D single-crystalline Ni_3S_4 nanosheet frames. To the best of our knowledge, the controlled-synthesis of the rigid 3D Ni_3S_4 nanosheet frames has not been reported. As a demonstration, the obtained 3D Ni_3S_4 nanosheet frames were used as the electrode of a supercapacitor. Its excellent electrochemical performance outperformed most of the nickel sulfides based electrodes from previous reports. We anticipate

that the unique 3D Ni_3S_4 structure originating from the ultrathin Ni_3S_4 nanosheet will enable us to further explore its intrinsic properties in the field of catalysis, cathode materials in lithium batteries, and so on.

In a typical reaction, a mixture of nickel stearate, oleic acid, n-dodecanethiol, and toluene was added in to a Teflon-lined stainless autoclave. After continuous stirring for 5 min, the reaction solution is heated up to 200 ^oC for 2.5 h. Once the reaction is finished and cooled down to room temperature, the black products precipitated at the bottom of the autoclave are purified with excess ethanol by centrifugation and then are easily dispersed in ethanol for further characterization.

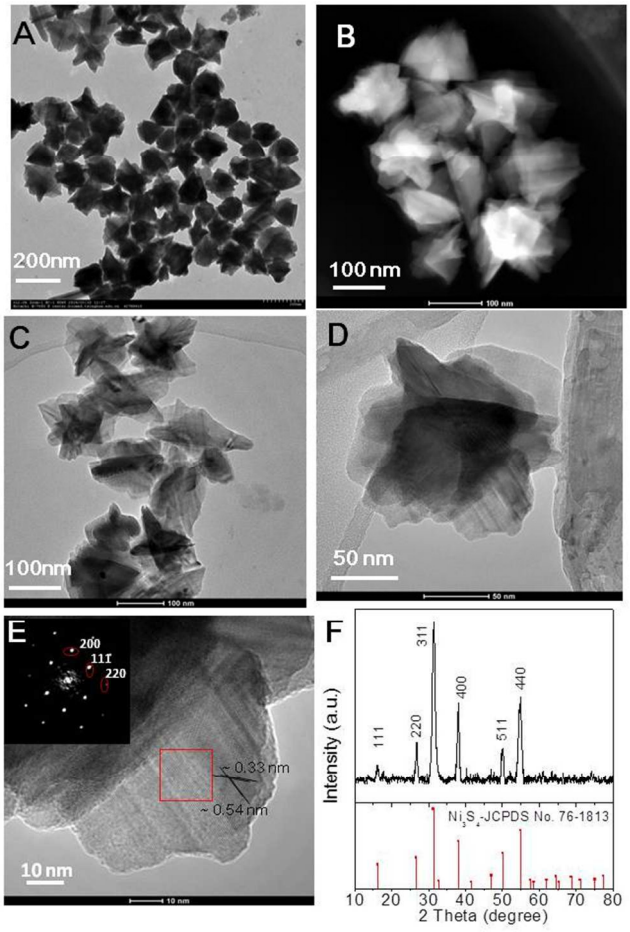

Fig. 1 TEM image (A), STEM image (B), HRTEM images (C, D, E), inset FFT and XRD pattern (F) of the 3D Ni_3S_4 nanosheet frames

Typical rigid 3D Ni_3S_4 nanosheet frames are displayed in Fig. 1. The size and morphology of the as-prepared frames were characterized by transmission electron microscopy (TEM). A panoramic view of 3D frames (Fig. 1A) reveals that the sample consists entirely of 3D frame structure with many ridges and vertices. The scanning transmission electron microscopy (STEM) (Fig. 1B) and the high resolution transmission electron microscope (HRTEM) images (Fig. 1C, 1D) show that the average size of the 3D nickel sulfide frames is ~160 nm and they were assembled from very thin Ni_3S_4 sheets. The crystallographic phase of the nickel sulfide nanostructures was investigated by X-ray diffraction (XRD) (Fig. 1F). The position of the diffraction peaks is in good accordance to the standard pattern of the cubic Ni_3S_4 (ICDD-JCPDS card no. 76-1813), indicating the sample consists of pure single crystalline Ni_3S_4. It is worth noting that the 3D structures result in an apparent enhancement on peak (311) and a decrease on peak (111) of Ni_3S_4 diffraction patterns. The single-crystalline feature of the Ni_3S_4 frames was further verified by HRTEM (Fig. 1E). The lattice spacing of ~0.54 and ~0.33 nm, matches well with the interplanar spacing of the (111) and (220) planes of the cubic Ni_3S_4, respectively. In addition, the selected area electron diffraction pattern from the edges shows strong Ni_3S_4 (111), (220) diffraction spots, corresponding to the d-spacing of 0.54 and 0.33 nm, respectively. These results clearly demonstrated that the 3D Ni_3S_4 frame composed of pure and single crystalline cubic Ni_3S_4 ultrathin nanosheets. It is notable that the obtained 3D Ni_3S_4 frames are very open but also rigid. No morphology change was observed after 30 min ultrasonication, further implying their good structural integrity and stability (Fig. S1).

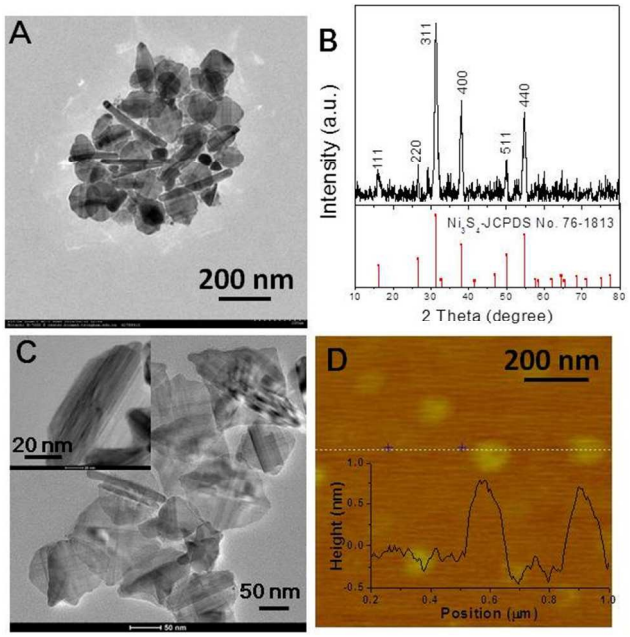

Fig. 2 TEM image (A), XRD pattern (B), HRTEM images (C), AFM image with height information data (D) of the flat Ni_3S_4 sheets

When the ratio of n-dodecanethiol/oleic acid (DDT/OA) in the reaction system was increased while keeping all the other parameters unchanged, relative flat nickel sulfide sheets were obtained. Fig. 2A shows a typical TEM image of the as-prepared nickel sulfide products, most of which exhibit sheet-like morphology. XRD pattern of the nickel sulfide sheets is similar to that of the Ni_3S_4 3D frames (Fig. 2B), except no decrease in the intensity of peak (111) of Ni_3S_4 diffraction patterns. The HRTEM images (Fig. 2C, 2D) reveal that the Ni_3S_4 sheets have near rectangular shape with average lateral size of ~130 nm. The thickness of the sheet was determined with atomic force microscope (AFM, Fig. 2D). Prominently, the thickness was measured to be only 1.0 nm.

Our experimental results imply that the ratio of DDT/OA plays an important role in tuning the structure of Ni_3S_4 since the only varying parameter in preparing 3D Ni_3S_4 frames and flat Ni_3S_4 sheets is the ratio of DDT/OA; n-dodecanethiol is also the source

of sulfur for the formation of Ni_3S_4. Controlled experiments were carried out to investigate the evolution of Ni_3S_4 sheets and 3D frames by varying the ratio of DDT/OA and the reaction time. The evolution of the morphology was examined by TEM, as shown in Fig. S2-4. At the medium ratio of DDT/OA (e.g., 0.6ml/6ml or 0.8ml/6ml), the final product is composed of both sheets and 3D frames (Fig. S2). For the sample prepared at the low ratio (e.g., 0.5ml/6ml) and collected at the early stage (0.5h, 1.0 h, 1.5 h) exhibits an immature 3D assembly structure, and the size and the sharpness of 3D structure is increased with the extension of time (Fig. S3). For the sample prepared at high ratio (e.g., 1ml/6ml) and collected at the early stage (0.5h, 1.0 h, 1.5 h) (Fig. S4) exhibits sheet structure, and the size of sheet is increased with the extension of time (Fig. S4). From the HRTEM image of a single relative small Ni_3S_4 3D frames (Fig. S5), the clear lattice fringes at extended end are visible and the interplane distance is measured as ~ 0.54 nm and ~ 0.29 nm, corresponding to the (111), (311) planes. This indicates the growth direction is along the [311] direction. The growth rate of {111} crystallographic facet was lower than that of the {311} facet, which is consistent with those intensity ratio for the (111) vs the (311) peak (Fig. 1F), in a qualitative manner. According to these observations and the previous literature,[16] we propose that both the Ni_3S_4 sheets and 3D frames could be obtained from the coalescence of the Ni_3S_4 nucleus (Scheme 1a) in an oriented way. At the initial stage, Ni_3S_4 nanopyramids (Scheme 1f) are formed in the reaction system. When the ratio of DDT/OA is low, the Ni_3S_4 nanopyramids tend to aggregate to minimize the total surface energy, and thus small Ni_3S_4 nano-aggregates are formed through a self assembly process (Scheme 1b). As the reaction continues, the growth rate of the {111} facets was lower than that of the {311} facets, which results in the growth along the [311] direction, and finally leads to the formation of Ni_3S_4 3D frames assembled from thin Ni_3S_4 nanosheets (Scheme 1c). On the other hand, the higher DDT/OA ratio results in well dispersed Ni_3S_4 nanopyramids initially (Scheme 1f). As the reaction goes on, the reaction system tends to minimize the total energy by forming relatively flat Ni_3S_4 sheets through the coordination of n-dodecanethiol and oleic acid (Scheme 1g). When the DDT/OA ratio is at a medium level, both 3D frames and relatively flat sheets are formed in the reaction system (Scheme 1e).

A good electrode material for a pseudocapacitor should have a large specific surface area and suitable pore-size distribution which allows efficient contact between the electroactive sites and the electrolyte ions for fast faradic energy storage.[17] Since the Ni_3S_4 3D frames are highly opened structure, they should have higher specific surface area than the stacked flat Ni_3S_4 sheets. Indeed, nitrogen adsorption/desorption analysis revealed that Ni_3S_4 3D frames have higher BET surface area (122.6 m^2 g^{-1}) than the flat Ni_3S_4 sheets (66.7 m^2 g^{-1}). The value is also higher than some other nickel sulfide nanomaterials reported in the literature, such as NiS hierarchical hollow microsphere (34.3 m^2 g^{-1}),[18] and hierarchical flower-like β -NiS nanostructure (24.0615 m^2 g^{-1}).[19] The nitrogen adsorption/desorption isotherm of the Ni_3S_4 3D frames (Fig. 3A) displays a type-IV isotherm with a type-H3 hysteresis loop in the relative pressure range of 0.6-1.0 p/p_0, indicating the presence of mesoporous structure. SEM images of the working electrode were shown in Fig. S6. As expected, the flat Ni_3S_4 nanosheets pack like a stack of paper with a smooth featureless surface. For the 3D Ni_3S_4 nanosheet frames, the surface has essentially indistinguishable microstructures. It shall be noted that there is free space inside each individual 3D nanosheet frames as well as between them.

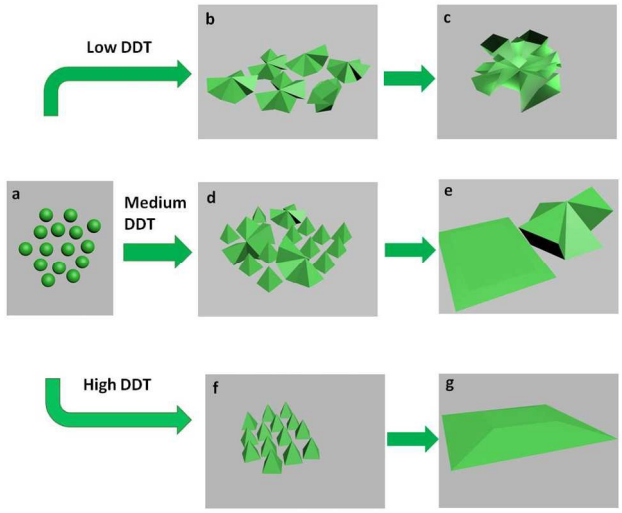

Scheme 1 Schematic illustration of the proposed mechanism for the formation of the 3D Ni_3S_4 nanosheet frames and Ni_3S_4 sheets

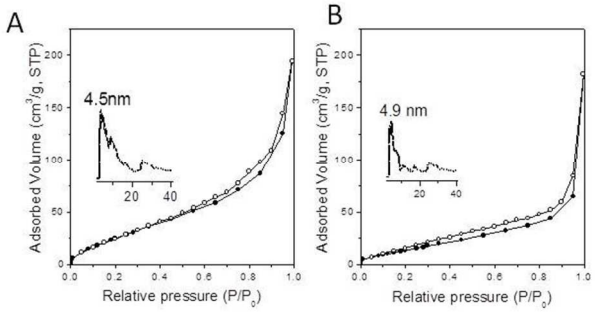

Fig. 3 N_2-sorption isotherms and pore size distribution (inset) of Ni_3S_4 3D frames (A) and flat Ni_3S_4 sheets (B)

The electrochemical properties of the Ni_3S_4 3D frames and flat Ni_3S_4 sheets were studied in 3M KOH aqueous solution using a three-electrode system. Their typical cyclic voltammetry (CV) curves at the scan rate of 5 mV s^{-1} are shown in Fig. 4A. There is a pair of redox peaks in the potential range of -0.15～0.55 V (vs. SCE). For nickel sulfide based electrodes, it is well accepted that the storage mechanism is mainly based on the surface redox reaction between Ni^{2+} and Ni^{3+}.[9, 11, 19] It is observed from the CV curves that the Ni_3S_4 3D frame electrode has higher electrochemical activity. The rate capability of the Ni_3S_4 3D frame based electrode is illustrated in Fig. S7A at different scan rates. With increasing scan rate, the shape of the curves was maintained, suggesting relatively good rate performance. The peak current increased and the oxidation peak shifted to a more positive position while the reduction peak shifted to a more negative position. This is due to the increased internal resistance within the pseudoactive material with an increase in scan rate.

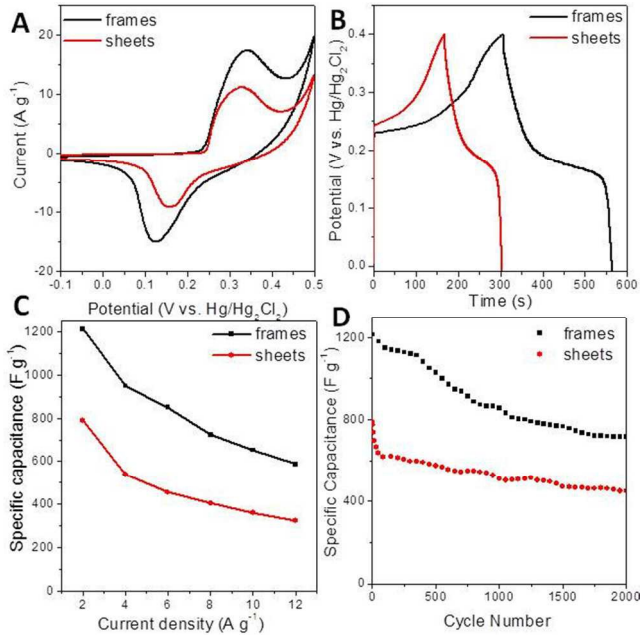

Fig. 4 The cyclic voltammogram curves at the scan rate of 5mV s^{-1} (A), the galvanostatic charge-discharge curves at a current density of 2 A g^{-1} (B), the specific capacitance as a function of current density (C), and the dependence of the discharge specific capacitance on the charge-discharge cycle numbers at a current density of 2.0 A g^{-1} (D) of the Ni_3S_4 3D frame electrode and the flat Ni_3S_4 sheet electrode, respectively.

Consistent with the CV results, the plateaus in the charge/discharge curves (Fig. 4B) indicate the existence of faradic processes. The ability for a high-rate discharge is crucial for a pseudocapacitor. Galvanostatic charge/discharge curves of the Ni_3S_4 3D frame based electrode at different current densities are shown in Fig. S7B and the corresponding rate dependent specific capacitance as a function of current density for Ni_3S_4 3D frame and Ni_3S_4 sheet based electrodes is shown in Fig. 4C. Ni_3S_4 3D frame electrode displayed a high capacitance of 1213 F g^{-1} and 587 F g^{-1} at the current densities of 2 A g^{-1} and 12 A g^{-1}, respectively. While the capacitance of Ni_3S_4 sheet electrode is only 789 F g^{-1} and 324 F g^{-1}, respectively. The specific capacitance of our Ni_3S_4 3D frame electrode is significantly larger than some nickel sulfide based electrodes from the previous studies, such as NiS hollow spheres (927 F g^{-1} at 4.08 A g^{-1}),[10] flower-like β -NiS (857.76 F g^{-1} at 2 A g^{-1}),[11] and NiS_2 nanocube (695 F g^{-1} at 1.25 A g^{-1}).[12] The good pseudocapacitive performance of Ni_3S_4 3D frame electrode could be attributed to its unique structural features. Specifically, the high surface area and open structure composed of ultrathin nanosheets can provide not only high interfacial area between the electrode material and the electrolyte, but also allow fast ionic diffusion.[22] Fig. 4D shows the cycling performance of as-prepared electrodes at a current density of 2 A g^{-1} in a voltage window of 0-0.4 V. The initial capacitance of Ni_3S_4 3D frame electrode is 1213 F g^{-1}, and around 60% of the initial capacitance was retained after 2000 cycles, indicating relatively high cycling stability. While the capacitance of Ni_3S_4 sheet electrode dropped to 449 F g^{-1} after 2000 cycles and around 56% of the initial capacitance was retained. The cycling performance of our Ni_3S_4 3D frame electrode is better than some nickel sulfide based electrodes from literature, such as NiS hollow spheres (52% retention after 2000 cycles),[10] and flower-like β -NiS (44% retention after 1000 cycles).[11] This improved capacitance retention may be attributed to the enhanced structural integrity of these rigid 3D Ni_3S_4 nanosheet frames which are stabilized by plastically deformed ridges.

Conclusions

In summary, a facile one-pot solvothermal method has been developed to prepare rigid 3D Ni_3S_4 nanosheet frames. The as-prepared 3D Ni_3S_4 nanosheet frames are shown to be very uniform in size with open and rigid structure. The DDT/OA ratio is shown to play an important role in altering the morphology of Ni_3S_4 nanostructure. Relatively flat Ni_3S_4 sheets were obtained with high DDT/OA ratio. In virtue of its unique structure, the 3D Ni_3S_4 nanosheet frame electrode exhibits high specific capacitances of 1213F g^{-1} at the current density of 2 A g^{-1}. Over 60% of the initial capacitances can be retained after 2000 cycles. This suggests its promising application as the electrode material for high-performance pseudocapacitors. Moreover, we anticipate that this simple solvothermal method can be extended to the synthesis of other 3D metal sulfide nanostructure.

Acknowledgements

We acknowledge funding by the NNSF (91123001, 21322105, and 51372025), the Research Fund for the Doctoral Program of Higher Education of China (2011101120016), Beijing Excellent Talent Project (2012D009011000007) and Program for New Century Excellent Talents in University (NCET-11-0793).

Notes and references

[a] *School of Materials Science & Engineering, Beijing Institute of Technology, Beijing 100081, P. R. China. Fax: +86-10-68918065; Tel: +86-10-68918065; E-mail: liujiajia@bit.edu.cn; zhangjt@bit.edu.cn*

[b] *Institute of Chemical and Engineering Sciences, A*STAR, 1 Pesek Road, Jurong Island 627833, Singapore.*

[c] *School of Chemical Engineering, The University of Queensland, St Lucia, Brisbane, QLD 4072, Australia.*

† Electronic Supplementary Information (ESI) available: [details of any supplementary information available should be included here]. See DOI: 10.1039/b000000x/

‡ Footnotes should appear here. These might include comments relevant to but not central to the matter under discussion, limited experimental and spectral data, and crystallographic data.

1 J. H. Han, S. Lee, and J. Cheon, *Chem. Soc. Rev.*, 2013, **42**, 2581; M. Gao, Y. Xu, J. Jiang and S. Yu, *Chem. Soc. Rev.*, 2013, **42**, 2986.

2 J. L. Mohanan, I. U. Arachchige and S. L. Brock, *Science*, 2005, **307**, 397; J. B. Rivest, R. Buonsanti, T. E. Pick, L. Zhu, E. Lim, C. Clavero, E. Schaible, B. A. Helms and D. J. Milliron, *J. Am. Chem. Soc.*, 2013, **135**, 7446.

3 J. Feng, X. Sun, C. Wu, L. Peng, C. Lin, S. Hu, J. Yang and Y. Xie, *J. Am. Chem. Soc.*, 2011, **133**, 17832; Y. Du, Z. Yin, J. Zhu, X. Huang, X. WU, Z. Zeng, Q. Yan and H. Zhang, *Nat. Commun.*, 2012, **3**, 1; Z. Zeng, T. Sun, J. Zhu, X. Huang, Z. Yin, G. Lu, Z. Fan, Q. Yan, H. H. Hng and H. Zhang, *Angew. Chem. Int. Ed.*, 2012, **51**, 9052; X. Zhang, J. Zhang, J. Zhao, B. Pan, M. Kong, J. Chen and Y. Xie, *J. Am. Chem. Soc.*, 2012, **134**, 11908; J. S. Son, X. Wen, J. Joo, J. Chae, S. Bake, K. Park, J. H. Kim, K. An, J. H. Yu, S. G. Kwon, S. Choi, Z. Wang, Y. Kim, Y. Kuk, R. Hoffmann and T. Hyeon, *Angew. Chem. Int. Ed.*, 2009, **48**, 6861.

4 J. Luo, H. D. Jang, T. Sun, L. Xiao, Z. He, A. P. Katsoulidis, M. G. Kanatzides, J. M. Gibson and J. Huang, *ACS Nano*, 2011, **5**, 8943.

5 Y. Li, Z. Li and P. K. Shen, *Adv. Mater.*, 2013, **25**, 2474; L. Zhang, S. Zhao, X. N. Tian and X. S. Zhao, *Langmuir*, 2010, **26**, 17624; L. Zhang, Z. Xiong and X. S. Zhao, *J. Power Sources*, 2013, **222**, 326.

6 S. Zhang, Y. Li and N. Pan, *J. Power Sources*, 2012, **206**, 476; J. Chen, K. Sheng, P. Luo, C. Li and G. Shi, *Adv. Mater.*, 2012, **24**, 4569; S. Yin, Z. Niu and X. Chen, *Small*, 2012, **8**, 2458 .

7 J. Luo, J. Kim and J. Huang, *Accounts Chem. Res.*, 2013, **46**, 2225; J. Luo, H. Jang and J. Huang, *ACS Nano*, 2013, **7**, 1464.

8 W. Wei, L. Mi, Y. Gao, Z. Zheng, W. Chen and X. Guan, *Chem. Mater.*, DOI: 10.1021/cm5006482 2000, **35**, 3523; J. Yang, C. Bao, K. Zhu, T. Yu, F. Li, J. Liu, Z. Li and Z. Zou, *Chem. Commun.*, 2014, **50**, 4832; C. Wei, Q. Lu, J. Sun and F. Gao, *Nanoscale*, 2013, **5**, 12224.

9 L. Hou, C. Yuan, D. Li, L. Yang, L. Shen and F. Zhang, *Electrochim. Acta*, 2011, **56**, 7254.

10 T. Zhu, Z. Wang, S. Ding, J. S. Chen and X. W. Lou, *RSC Adv*, 2011, **1**, 397.

11 J. Yang, X. Duan, Q. Qin and W. Zheng, *J. Mater. Chem.*, 2013, **1**, 7880.

12 H. Pang, C. Wei, X. Li, G. Li, Y. Ma, S. Li, J. Chen and J. Zhang, *Scientific Reports*, 2013, **4**, 3577.

13 N. Mahmood, C. Zhang and Y. Hou, *Small*, 2013, **9**, 1321; X. Jiang, Y. Xie, J. Lu, L. Zhu, W. He and Y. Qian, *Adv. Mater.*, 2001, **13**, 1278; Y. Hu, J. Chen, W. Chen, X. Lin and X. Li, *Adv. Mater.*, 2003, **15**, 726.

14 G. Kullerud and R. A. Yund, *J. Petrology*, 1962, **3**, 126.

15 A. L. Abdelhady, M. A. Malik, P. O'Brien and F. Tuan, *J. Phys. Chem. C*, 2012, **116**, 2253; Q. Liu, A. Diaz, A. Prosvirin, Z. Luo and J. D. Batteas, *Nanoscale*, 2014, **6**, 8935.

16 C. Schliehe, B. H. Juareze, M. Pelletier, S. Jander, D. Greshnykh, M. Nagel, A. Merer, S. Foerster, A. Kornowski, C. Klinke and H. Weller, *Science* 2010, **329**, 550; J. Li, Z. Chen, Y. Hu, X. Wang, T. Zhang, W. Chen and Q. Wang, *J. Am. Chem. Soc.*, 2013, **125**, 1213.

17 X. Zhang, W. Shi, J. Zhu, W. Zhao, J. Ma, S. Mhaisalkar, T. L. Maria, Y. Yang, H. Zhang, H. H. Hng and Q. Yan, *Nano Res.*, 2010, **3**, 643; H. Wan, J. Jiang, J. Yu, K. Xu, L. Miao, L. Zhang, H. Chen and Y. Ruan, *CrystEngComm*, 2013, **15**, 7649.

18 Y. Wang, Q. Zhu, L. Tao and X. Su, *J. Mater. Chem.*, 2011, **21**, 9248.

19 W. We, L. Mi, Y. Gao, Z. Zheng, W. Chen and X. Guan, *Chem. Mater.*, 2014, **26**, 3418.